Energy Advances

ROYAL SOCIETY OF CHEMISTRY

PAPER

View Article Online
View Journal | View Issue

Cite this: *Energy Adv.*, 2024, 3, 2399

Synthesis of dendrimer stabilized high-density silver nanoparticles on reduced graphene oxide for catalytic and antibacterial properties†

Thi Nhat Thang Nguyen,[a] Subodh Kumar *[b] and Xuan Thang Cao *[a]

Received 5th May 2024,
Accepted 24th July 2024

DOI: 10.1039/d4ya00284a

rsc.li/energy-advances

Immobilization of metal nanoparticles (MNPs) with high density on a solid support is a crucial approach for their facile recovery and to counter aggregation problems. We have developed a simple technique by mediating the Diels–Alder "click reaction" using a deep eutectic solvent (DES) system. In this method, maleic anhydride (MA) was first covalently grafted onto the surface of reduced graphene oxide (rGO), which is further utilized as a seeding platform to grow dendrimers through the consecutive reactions of ethylenediamine (EDA) and MA. Finally, silver nanoparticles (AgNPs) were deposited in high density onto the dendrimers through visible light photoreaction. This method has excluded the use of harmful chemicals and an external reductant for the functionalization of rGO and deposition of AgNPs, respectively. Moreover, we have investigated the effect of dendrimers' chain branching on the loading of AgNPs and evaluated their compound influence on the nitro-reduction reaction and antibacterial properties.

Introduction

Metal nanoparticles (MNPs) are known to be effective heterogeneous catalysts for various reactions due to their comparatively high activity and selectivity.[1,2] However, their uniform synthesis requires stabilizers in order to prevent the high attraction between the nanoparticles resulting in their aggregation. Therefore, the deposition of MNPs onto a solid surface is a well-known strategy to counter the aforementioned limitations and their facile recyclability.[3,4] Various catalyst synthesis techniques involve diverse heterogeneous supports such as graphitic carbon nanomaterials,[5,6] biopolymers,[7,8] nitrides,[9,10] metal oxides,[11] and organic polymers.[12] Reduced graphene oxide (rGO) is a 2D nanocarbon material synthesized through the reduction of graphene oxide (GO) and exfoliation reactions.[13,14] rGO layers are composed of sp^2 and sp^3-hybridized carbon atoms arranged in a hexagonal lattice.[15,16] The ratio of sp^2 and sp^3 carbon atoms can influence the chemical reactivity, electronic properties, dispersibility and compatibility with a wide range of organic and inorganic materials. Moreover, its exceptional mechanical strength, high surface area, ease of functionalization (covalent bonding, doping, or adsorption), and tunability make it a versatile carbon support.[17] The deposition of MNPs on the surface of rGO *via* various approaches is well documented.[18] However, controlling and uniformly loading MNPs, as well as ensuring their stability, is always a matter of further research.[19] Generally, MNPs tend to agglomerate during their deposition on solid supports and thus require some additional stabilizers.[20] These stabilizers can not only affect their catalytic performance but are also difficult to remove. Consequently, the functionalization approach has been one of the most utilized approaches to counter such obstacles.[21–23] Functionalization of support materials with desired functionalities or vacancies serves as an anchoring point to bind the metal salts in high density and suppress their agglomeration during the reduction process. There are different organic moieties (molecules/polymers) bearing the desired functional groups that have been used for the functionalization of solid supports.[24] These organic moieties have their own importance and features and can influence not only the deposition and loading of MNPs but also the reaction productivity accordingly. Dendrimers are the branched long chains polymers of repeated organic molecules and thus can be designed with tunable functionality and chain length.[25,26] These features can determine the final properties of the materials such as dispersibility, surface area, acidic–basic nature, electronic properties, binding affinity, selectivity, and biocompatibility.[27,28] Subsequently, they have been implemented in various fields such as catalysts, electrocatalysis, drug delivery, diagnostics, separations, and sensors.[29–34] Moreover, dendrimers can also control the size and stabilization of deposited MNPs.[35] Therefore, covalent growth of dendrimers onto the surface of rGO has provided a

[a] *Faculty of Chemical Engineering, Industrial University of Ho Chi Minh City, Vietnam. E-mail: caoxuanthang@iuh.edu.vn*
[b] *Department of Inorganic Chemistry, Faculty of Science, Palacký University, Olomouc 779 00, Czech Republic. E-mail: subodh.kumar@upol.cz*

† Electronic supplementary information (ESI) available. See DOI: https://doi.org/10.1039/d4ya00284a

great opening for the MNP deposition and their subsequent application in different fields.[36] In addition, incorporation of dendrimers imparts additional functionality thus further expanding its utility in activation and absorption of reaction substrates.[37] However, covalent immobilization of dendrimers onto the rGO surface generally requires tedious chemical processes for the effective growth of dendrimers in terms of loading.[38] These processes are energy intensive and require harmful chemicals and reductants. Direct covalent immobilization of organic moieties through the Diels–Alder "click" reaction directly utilizing the >C=C< double bonds of rGO could result in high loading without involving any external organic linkers. However, this transformation needs to be performed under mild reaction conditions for the benefit of the environment. Deep eutectic solvents (DESs) are a new class of room temperature ionic liquids and have been evident as an unprecedented catalytic medium for facilitating several organic reactions, including the Diels–Alder "click" reaction.[39–42]

In this study, we have leveraged the feature of DESs to perform a "click" reaction for the initial covalent functionalization of rGO with maleic anhydride (MA) under ultrasound, thereby avoiding harmful organic solvents as well as reducing energy intensive processes (Scheme 1). Moreover, consecutive reactions were conducted at room temperature and finally silver nanoparticles (AgNPs) were deposited using a visible light induced photoreduction process. Subsequently, the synthesized materials were tested for nitro-reduction reaction and antibacterial activity.

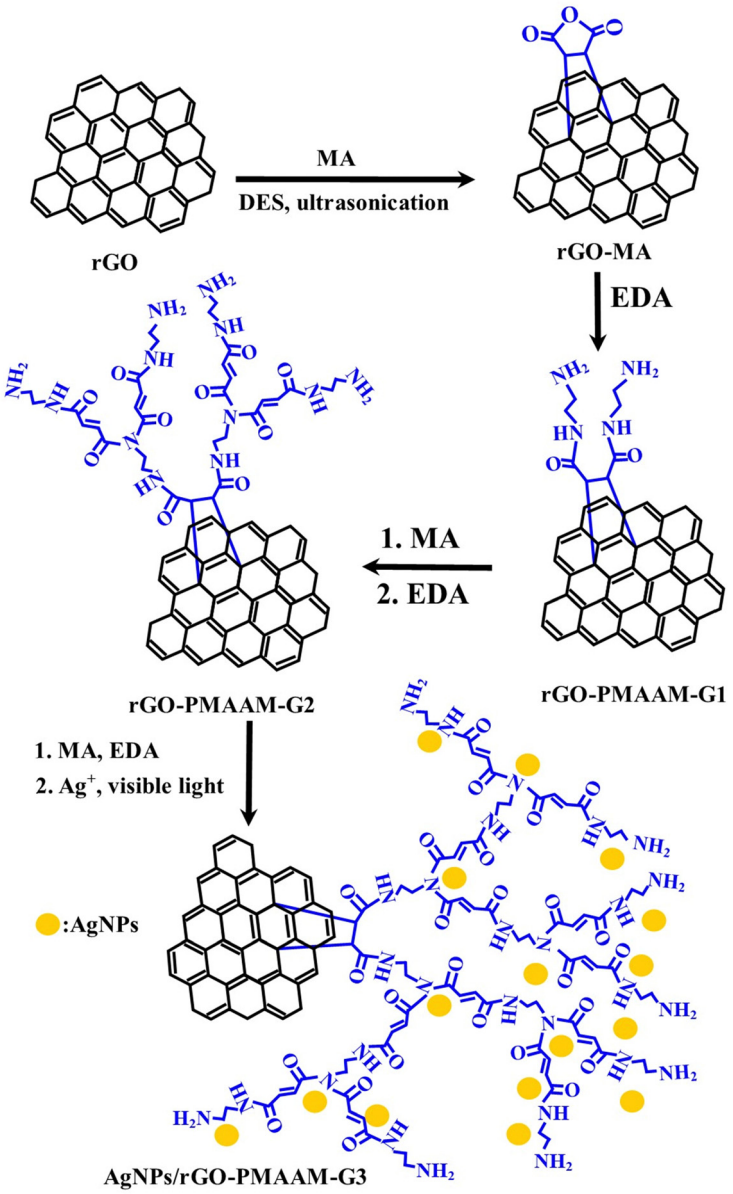

Scheme 1 Preparation of the AgNPs/rGO-PMAAM dendrimer.

Experiment

Materials

Graphite powder with a particle size of 50 μm was purchased from Loba Chemie Pvt. Ltd, India. Maleic anhydride (MA), choline chloride (ChCl), zinc chloride ($ZnCl_2$), ethylene diamine (EDA), and silver nitrate were procured from Merck, Vietnam. All the solvents and chemicals were used without further purification. Deionized water was used in all the experiments.

Characterization techniques

FTIR spectra were examined using a Bruker Tensor 27 (Germany) spectrometer in the range of 4000–500 cm^{-1}. Diffractograms were recorded on a Shimadzu 6100 X-ray diffractometer (Japan) using Cu Kα radiation (λ = 1.5406 Å) at a voltage of 40 kV, and a current of 30 mA. Raman spectroscopy was conducted using a LabRAM spectrometer (HORIBA Jobin Yvon, Edison, NJ) with a 785 nm diode laser. The surface morphologies of the synthesized samples were determined with a scanning electron microscope (SEM) connected with an EDX spectrometer (Hitachi JEOL-JSM-6700F system, Japan). Silver nanoparticles were characterized by transmission electron microscopy (TEM) using a Hitachi H-7500 instrument operating at 80 kV. UV-vis spectra were recorded in solution form over the wavelength range of 200–800 nm using a UV-vis spectrophotometer (METASH, China).

Synthesis of maleic anhydride functionalized reduced graphene oxide (rGO-MA)

rGO and DES were prepared as described in our previous study.[43] rGO (100 mg) was first dispersed in a mixture of DES (3.0 g) and deionized water (3.0 mL), and then maleic anhydride (MA, 800 mg) was added. The resulting suspension was ultrasonicated at 65 °C for 8 h for the Diels–Alder ''click'' reaction to occur between MA and rGO. The final material was filtered, washed several times (water and methanol) and finally vacuum dried to afford the rGO-MA composite.

Synthesis of dendrimer functionalized reduced graphene oxide (rGO-PMAAM)

The as-prepared rGO-MA (130 mg) was dispersed in methanol (5.0 mL) with the help of an ultrasonicator at room temperature. N_2 gas was flushed many times through this dispersion and then ethylenediamine (EDA) (2.0 mL) was slowly injected using a syringe while continuously stirring, and the resulting mixture was left overnight. The synthesized material (rGO-PMAAM-G1) was centrifugally separated, washed with ethanol, and dried at 45 °C. For the synthesis of rGO-PMAAM-G2, a mixture of MA (200 mg) in methanol (2.5 mL) was added into the dispersion of rGO-PMAAM-G1 (165 mg) in methanol (2.5 mL) while stirring under an inert atmosphere overnight. This washed and dried material was used to prepare rGO-PMAAM-G2 *via* the same way as for rGO-PMAAM-G1 through the reaction of EDA. Finally, rGO-PMAAM-G3 was prepared by following the same procedure as above.

Deposition of silver nanoparticles (AgNPs) on rGO-PMAAM

AgNPs/rGO-PMAAM are synthesized by the reaction of different rGO-PMAAM and silver ions *via* photoreaction under visible light irradiation. First, rGO-PMAAM (0.02 g) was dispersed in dimethylformamide (DMF, 15.0 mL) and then 10.0 mL of $AgNO_3$ (0.1 N) was added dropwise under stirring to anchor the silver ions onto the functional groups of the dendrimers. Next, the resulting mixture was centrifuged and washed to remove the unanchored silver salt. The same material was further dispersed in DMF and placed in a chamber illuminated under a visible light (xenon lamp) with wavelengths from 400 to 800 nm for 2 h. Finally, the product was filtered, rinsed with water and ethanol to remove residual unsupported Ag species, and finally dried at 45 °C until reaching a constant weight to afford the respective AgNPs/rGO-PMAAM materials.

Catalytic activity of AgNPs/rGO-PMAAM materials

The catalytic activity of the synthesized materials was tested for the reduction of 4-nitrophenol (4-NP) into 4-aminophenol (4-AP). The reaction was conducted in a quartz cuvette by taking 2.0 mL of 4-NP solution of 1.0 mM, 1.0 mL of 0.1 M $NaBH_4$ solution and 1.0 mg of the respective AgNPs/rGO-PMAAM-G materials. The variation in 4-NP concentration over time was determined by using a UV-vis spectrophotometer. The characteristic absorption peaks of 4-NP and 4-AP at 400 and 300 nm, respectively, were used to evaluate the performance of the catalysts. We further investigated the reusability of the recovered catalysts after the reaction for the next five cycles.

Bioactivity test of the AgNPs/rGO-PMAAM materials

We followed a disk diffusion method to investigate the antimicrobial properties of AgNPs/rGO-PMAAM nanomaterials against pathogenic bacterial strains by taking dimethyl sulfoxide (DMSO) as the negative control and streptomycin antibiotic as the positive control. Aliquots (100 μL) of each bacterium with a cell density of 10^6 CFU mL^{-1} were piped out and then evenly spread on the surface of agar plates by using a sterile cotton swab and left for drying. After that, 50 μL of streptomycin (0.1 mg mL^{-1}) and 50 μL of AgNPs/rGO-PMAAM-G (1.5 mg mL^{-1}) in DMSO were placed to the agar plates which was transferred to the refrigerator (10 °C) for about 4–8 h for the diffusion process and then the temperature was increased to 37 °C and the sample was left for the next 24 h. The samples were diluted with DMSO solution ranging from 0.1875 to 3.0 mg mL^{-1} to investigate the minimum inhibitory concentration (MIC) values.

Results and discussions

''Click'' reaction mediated covalent grafting of dendrimers and subsequent deposition of AgNPs were performed involving a DES and visible light photo reaction, respectively. Raman and FTIR spectroscopic techniques were implemented to confirm the successful covalent interaction between MA and rGO in the first step, and the subsequent growth of dendrimers. Raman

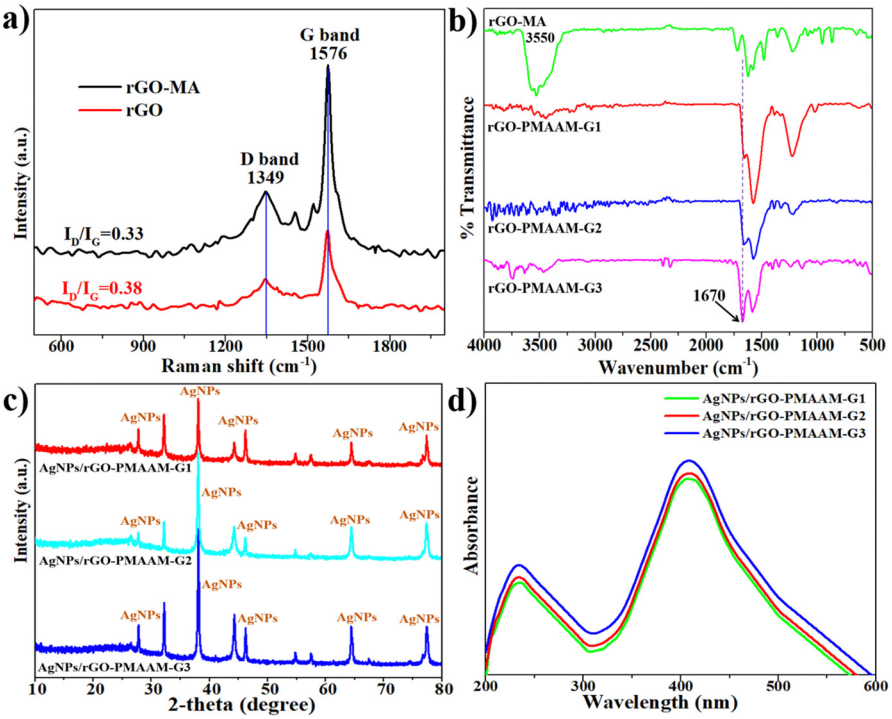

Fig. 1 (a) Raman spectra of rGO and rGO-MA; (b) FT-IR spectra of rGO-MA, rGO-PMAAM-G1, rGO-PMAAM-G2, and rGO-PMAAM-G3; (c) diffractograms of AgNPs/rGO-PMAAM-G1, AgNPs/rGO-PMAAM-G2, and AgNPs/rGO-PMAAM-G3; (d) UV-vis spectra of AgNPs/rGO-PMAAM-G1, AgNPs/rGO-PMAAM-G2 and AgNPs/rGO-PMAAM-G3.

spectroscopy has shown two characteristic peaks at 1349 cm^{-1} (D band) and 1576 cm^{-1} (G band). The D-peak is derived from the transition of C=C (sp^2) to C–C (sp^3) hybridization and reveals the degree of defects in the rGO materials. The sp^3/sp^2 carbon ratio was calculated to be 0.33 and 0.38 for rGO and rGO-MA, respectively, indicating the formation of a higher number of C-sp^3 bonds after DA reaction. These results confirm the successful covalent functionalization of MA onto the rGO surface (Fig. 1a). Moreover, the FT-IR spectrum of rGO-MA indicated peaks at 1580 and 1725 cm^{-1} corresponding to the C=C bonds in the aromatic region and >C=O stretching of the anhydride group, respectively. Moreover, after reaction with ethylenediamine (EDA), a new peak at 1670 cm^{-1} appeared, indicating the formation of the –CO–NH bond. Notably, the peak intensities of these functional groups (C=O stretching of anhydride and –CO–NH–) seemed to be increased successively after each respective attachment of MA and EDA. These results further confirmed that MA and EDA have been covalently functionalized in their respective manners to grow superb-ranched dendrimers on the rGO surface. Additionally, we have utilized a thermogravimetric analysis (TGA) method to confirm the successful synthesis of rGO-MA and rGO-PMAAM-G materials (Fig. S2, ESI†). Thermograms of the respective materials have shown successive weight loss in the temperature range of 50–800 °C. The initial weight loss could be due to the trapped moisture and decomposition of residual oxygen-containing functional groups on the surface of rGO. rGO-MA was found to be the most thermally stable resulting in a residual weight of 65%. However, the residual weight for rGO-PMAAM-G1, rGO-PMAAM-G2, and rGO-PMAAM-G3 was 53, 48 and 39%, respectively. These results clearly implied that the polymer chain length reduced the thermal stability of the respective materials. Moreover, the successive variation in their thermal stability profiles clearly demonstrates the successful functionalization of MA and EDA to form branched dendrimers on the surface of rGO.

X-ray diffractograms of rGO, rGO-PMAAM-G1, rGO-PMAAM-G2, rGO-PMAAM-G3, AgNPs/rGO-PMAAM-G1, AgNPs/rGO-PMAAM-G2, and AgNPs/rGO-PMAAM-G3 are presented in Fig. 1 and Fig. S1 (ESI†). rGO has a diffraction peak at 2θ = 26.6° attributed to the characteristic face (002), corresponding to a lattice spacing d = 0.34 nm between the graphite crystal planes (Fig. S1a, ESI†). The same characteristic peak has shifted to a lower value demonstrating an increase in the d-value due to the covalent grafting of MA and EDA. Moreover, new peaks appeared at diffraction angles (2θ values) of 27°, 32°, 38.5°, 44°, 64.5°, and 77.5° for the lattice surfaces (210), (122), (111), (200), (220), and (311), respectively (Fig. 1c), after integrating the AgNPs on the surface of respective materials, and were found to be the characteristic diffraction pattern of AgNPs. The highest diffraction peaks of AgNPs/rGO-PMAAM-G1, AgNPs/rGO-PMAAM-G2, AgNPs/rGO-PMAAM-G3 at an angle of 2θ = 38.5° indicate that the crystals have a preferred growth direction in the plane with a Miller index (111). The average crystal sizes of AgNPs/rGO-PMAAM-G1, AgNPs/rGO-PMAAM-G2, and AgNPs/rGO-PMAAM-G3 were calculated to be 6.9, 8.4, and 9.7 nm, respectively, using the Debye–Scherrer equation ($d = 0.9\lambda/\beta\cos\theta$), where the full width at half maximum (FWHM) of the

diffraction peak in the (111) plane was determined. It is evident that as the length of the dendrimer chains increased, the average crystal size of AgNPs also increased. This could be due to the enhanced anchoring of metal salts at numerous functional groups and their subsequent reduction, leading to the formation of larger AgNPs. Furthermore, UV-vis spectroscopy of the materials shows two main characteristic peaks at wavelengths of 240 and 410 nm. The later peak at 410 nm is due to the formation of AgNPs and corresponds to their plasmonic nature hence proving the successful synthesis of AgNPs/rGO-PMAAM-G materials (Fig. 1d). Scanning electron microscopy (SEM) analysis was conducted to evaluate morphological changes in the materials (Fig. S3a and b, ESI†). The SEM results show that AgNPs/rGO-PMAAM-G3 seem to have obvious layered morphology. However, the surface has been changed in terms of crumbliness indicating the growth of dendrimer onto the rGO surface. Although AgNPs were not clearly identified, likely due to their small size and being obscured under layers, as well as the limitations of SEM. Moreover, a size distribution graph for AgNPs has been drawn from the TEM image (Fig. S3c inset, ESI†). The average size of AgNPs was calculated to be approximately 9.62 nm, which correlates well with the XRD data. Additionally, EDX spectroscopy results clearly showed the presence of silver element in the AgNPs/rGO-PMAAM-G1 and AgNPs/rGO-PMAAM-G3 (Fig. S4, ESI†). EDX analysis clearly shows that the atomic percentages of Ag in these two materials are 6.26% and 7.84%, respectively. The higher content of Ag in AgNPs/rGO-PMAAM-G3 confirms greater deposition compared to the rGO-PMAAM-G1 material. This could be due to the presence of more branched structures containing a higher number of oxygen and nitrogen functional groups. This is further supported by changes in the atomic percentages of carbon (C), oxygen (O), and nitrogen (N). Specifically, AgNPs/rGO-PMAAM-G1 showed atomic percentages of 79.06% C, 8.68% O, and 5.45% O, whereas AgNPs/rGO-PMAAM-G3 showed 67.70% C, 13.25% O, and 10.60% N. The increase in N and O atomic percentages suggests successful covalent grafting of MA and EDA thus confirming the growth of new branches.

We have investigated the effect of dendrimer chain branching on the catalytic ability of the respective materials, AgNPs/rGO-PMAAM-G1, AgNPs/rGO-PMAAM-G2, and AgNPs/rGO-PMAAM-G3, for the reduction of 4-NP under the conditions described in the Experimental section. Upon addition of

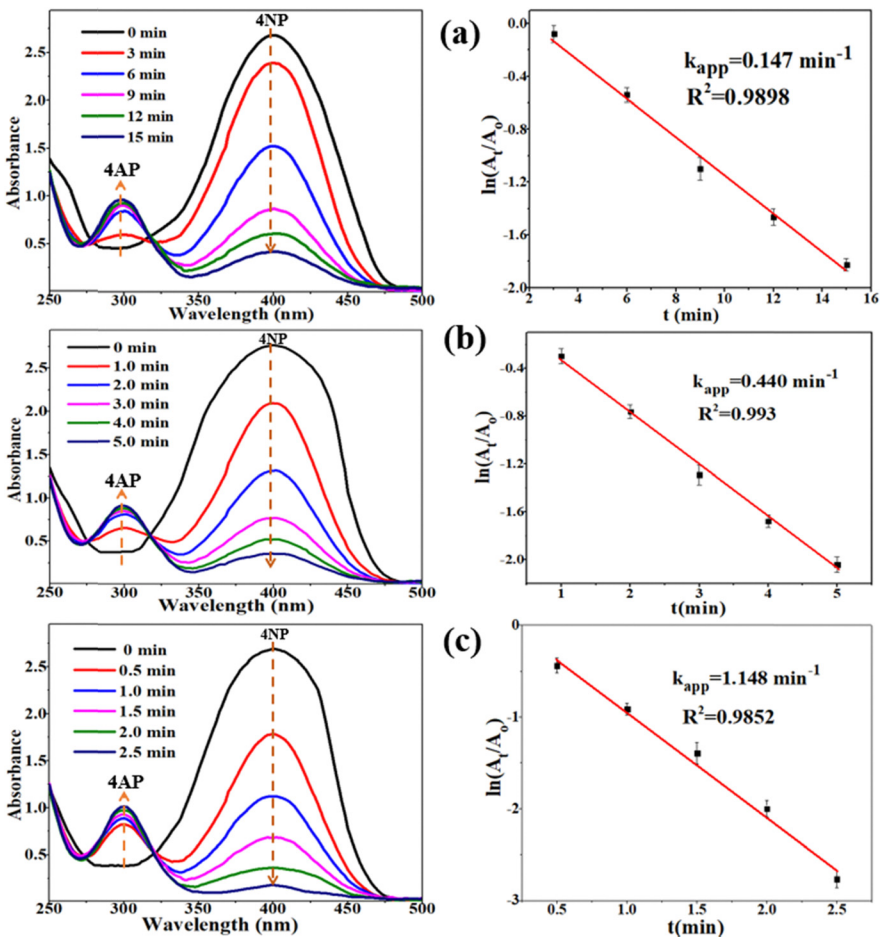

Fig. 2 UV-vis spectra and kinetics of 4-NP solution over time in the simultaneous presence of $NaBH_4$ and AgNPs/rGO-PMAAM-G1 (a), AgNPs/rGO-PMAAM-G2 (b), and AgNPs/rGO-PMAAM-G3 (c).

AgNPs/rGO-PMAAM catalysts, the dark yellow color mixture of 4-NP and $NaBH_4$ immediately fades and gradually turns colorless, signifying the reduction of 4-NP to 4-AP. UV-vis spectroscopy was used and recorded the gradual decrease in the intensity of the absorption peak of 4-NP at 400 nm and the gradual emergence of a new peak at 300 nm corresponding to the 4-AP over a time period (Fig. 2). AgNPs/rGO-PMAAM-G1, AgNPs/rGO-PMAAM-G2, and AgNPs/rGO-PMAAM-G3 took 15 minutes, 5 minutes, and 2.5 minutes to achieve 94.71, 96.24 and 99.68% reduction of 4-NP, respectively. This result demonstrates that the reduction efficiency increases with the length of the polymer chains. Thus, AgNPs/rGO-PMAAM-G3 has achieved the highest 4-NP reduction efficiency followed by AgNPs/rGO-PMAAM-G2 and AgNPs/rGO-PMAAM-G1. Furthermore, we investigated the kinetics of the reduction reaction. Based on the experimental results obtained, the kinetics of the 4-NP reduction reaction followed a first-order kinetic model with a relatively high linear regression coefficient ($R^2 > 0.985$). The values of the reaction rate constant were found to be gradually increased from 0.147 min^{-1} to 1.148 min^{-1} when using AgNPs/rGO-PMAAM-G1, AgNPs/rGO-PMAAM-G2, and AgNPs/rGO-PMAAM-G3, respectively. This can be explained by the fact that the formation of a higher number of stabilized AgNPs on the easily accessible and abundant N- and O-functionalities present in the superbranched dendrimer structure (high number and long chains) on the surface of rGO resulted in higher reaction rates.

The recycling study of the AgNPs/rGO-PMAAM-G3 catalyst was carried out to assess its stable nature under the reaction conditions (Fig. S5, ESI†). It is clearly observed that the reduction efficiency of AgNPs/rGO-PMAAM-G3 materials was maintained even after five cycles indicating the high stability of the AgNPs on its surface. After the fifth reuse, AgNPs/rGO-PMAAM-G3 retained a reduction efficiency of 89.1%. These results demonstrated that AgNPs/rGO-PMAAM-G3 is fully reusable, and the highly branched dendrimers can effectively stabilize more AgNPs thus exhibiting superior activity. Moreover, we performed XRD measurements of the reused AgNPs/rGO-PMAAM-G3 catalyst to investigate any changes in the material. The XRD diffractogram showed all the characteristic peaks of AgNPs confirming their existence and excluding the possibility of Ag leaching during the reaction (Fig. S6, ESI†).

In order to broaden the scope, we also investigated the antimicrobial properties of the two synthesized materials against three types of bacteria. The test results of AgNPs/rGO-PMAAM-G1 and AgNPs/rGO-PMAAM-G3 materials at a concentration of 1.0 mg L^{-1} were examined against three types of bacteria; Gr (+) bacteria: *Staphylococcus aureus* and *Bacillus cereus*; and Gr (−) bacteria: *Escherichia coli*. Based on the antimicrobial ring measurement for Gr (−) *Escherichia coli* as shown in Fig. 3a, the inhibition zone of AgNPs/rGO-PMAAM-G3 is 6.9 ± 0.5 mm in diameter which is larger than the 6.1 ± 0.5 mm of streptomycin and 5.2 ± 0.5 mm of AgNPs/rGO-PMAAM-G1. The results indicate that the antimicrobial ability

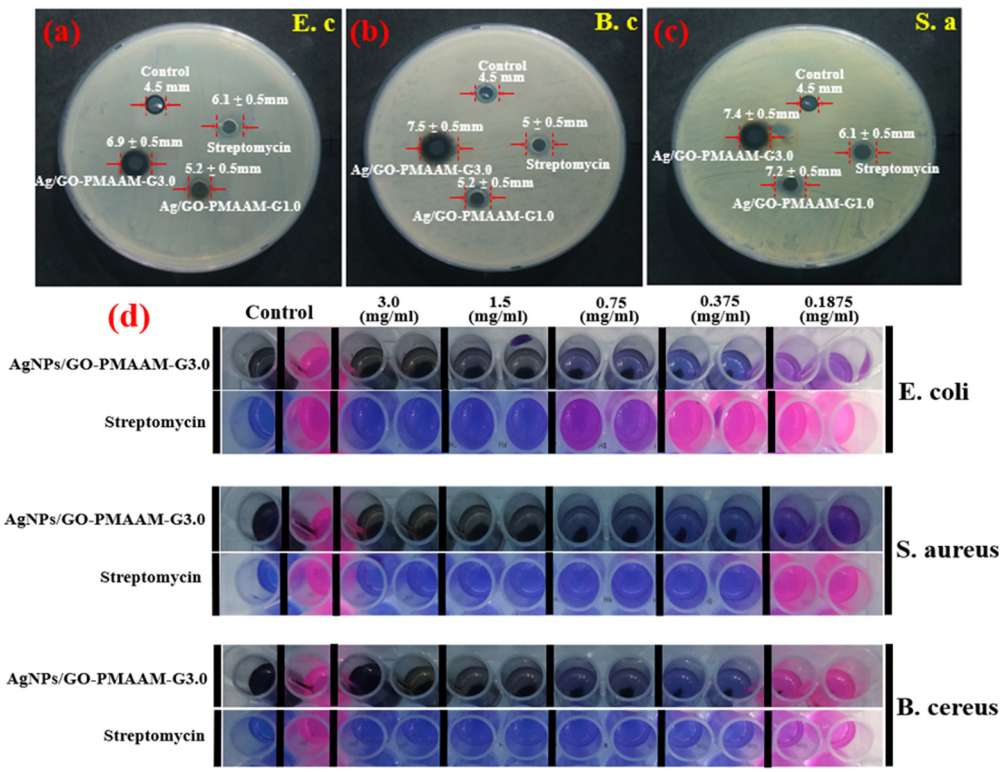

Fig. 3 Antibacterial capacity towards Gr (−) *Escherichia coli* (a), Gr (+) *Bacillus cereus* (b), and Gr (+) *Staphylococcus aureus* (c) of AgNPs/rGO-PMAAM-G1 and AgNPs/rGO-PMAAM-G3; MIC results of AgNPs/rGO-PMAAM-G3 (d) towards Gr (−) *Escherichia coli*, Gr (+) *Staphylococcus aureus*, and Gr (+) *Bacillus cereus*.

of AgNPs/rGO-PMAAM-G3 is undoubtedly superior to both streptomycin and AgNPs/rGO-PMAAM-G1. Similarly, against Gr (+) *Bacillus cereus*, AgNPs/rGO-PMAAM-G3 showed an inhibition zone of 7.5 ± 0.5 mm, compared to 5 ± 0.5 mm for streptomycin and 5.2 ± 0.5 mm for AgNPs/rGO-PMAAM-G1, indicating that dendrimers with branched chains attaching more AgNPs help to enhance their antimicrobial effectiveness (Fig. 3b). However, the antimicrobial ring diameter of AgNPs/rGO-PMAAM-G3 (7.4 ± 0.5 mm) is almost comparable to that of AgNPs/rGO-PMAAM-G1 (7.2 ± 0.5 mm) but better than streptomycin (6.1 ± 0.5 mm) for *Staphylococcus aureus* (Fig. 3c). The results of the antimicrobial ring measurements demonstrate that AgNPs/rGO-PMAAM-G3 composites possess superior antimicrobial properties compared to commercial streptomycin. MIC tests were conducted towards *Escherichia coli*, *Staphylococcus aureus*, and *Bacillus cereus*, and the results are shown in Fig. 3d. Based on the results, AgNPs/rGO-PMAAM-G3 showed the superior performance with MIC values of 0.1875 mg mL^{-1} against *Escherichia coli* and *Staphylococcus aureus*, compared to 0.75 mg mL^{-1} and 0.375 mg mL^{-1} for streptomycin, respectively. However, antimicrobial resistances were almost similar for AgNPs/rGO-PMAAM-G3 and streptomycin towards *Bacillus cereus* at a concentration of 0.375 mg mL^{-1}. The superior antimicrobial activity of AgNPs/rGO-PMAAM-G3 could be attributed to the increased surface area and enhanced interaction of dendrimer-attached AgNPs with bacterial cells. The dendrimer structure allows a higher loading of AgNPs, which in turn might be contributing to greater disruption of bacterial cell walls and membranes.[44,45] Additionally, the generation of reactive oxygen species (ROS) by AgNPs can lead to oxidative stress in bacteria, thus further enhancing their antimicrobial efficacy.[46,47] Our current study provides valuable insights into the antimicrobial properties of AgNPs/rGO-PMAAM composites. Moreover, future research can be focused on kill-time assays, antibiofilm activity evaluations, and in-depth mechanistic studies to fully elucidate the antimicrobial action of such materials. These studies will help in understanding the time-dependent killing kinetics, ability to prevent and disrupt biofilms, and the specific pathways through which the materials exert their antibacterial effects.

Conclusions

We have successfully performed the covalent grafting of dendrimers onto the rGO surface *via* the Diels–Alder "click" reaction using DESs and subsequently deposited AgNPs through visible light photoreaction. The synthesized nanocomposites were analyzed using modern analytical methods such as FT-IR spectroscopy, Raman spectroscopy, UV-vis spectroscopy, XRD, TGA, SEM-EDX elemental mapping, and TEM. The results of the measurements not only clearly showed that MA and EDA were functionalized, respectively, onto the rGO surface to grow dendrimers but also confirmed the successful deposition of AgNPs by the reduction of $AgNO_3$ under visible light. It was observed that more branched dendrimers were found to bind a higher amount of AgNPs and thus exhibited higher catalytic activity for the 4-NP reduction reaction accordingly. The kinetics of the reduction reaction followed a first-order kinetic model with a relatively high linear regression coefficient ($R^2 > 0.985$). Moreover, the catalysts showed excellent recyclability without a significant decrease in catalytic activity. We further tested the materials for their antibacterial activity against three bacterial strains: *Escherichia coli*, *Staphylococcus aureus* and *Bacillus cereus* and found that the higher density of AgNPs led to better antibacterial activity.

Data availability

The data that support the findings of this study are available in the ESI† of this article.

Conflicts of interest

There are no conflicts to declare.

Acknowledgements

This research was funded by the Industrial University of Ho Chi Minh City. S. K. acknowledges financial support from institutional sources of the Department of Inorganic Chemistry, Palacký University Olomouc, Czech Republic.

Notes and references

1 S. Navalon, A. Dhakshinamoorthy, M. Alvaro and H. Garcia, *Coord. Chem. Rev.*, 2016, **312**, 99–148.
2 C. Gao, F. Lyu and Y. Yin, *Chem. Rev.*, 2020, **121**, 834–881.
3 N. J. S. Costa and L. M. Rossi, *Nanoscale*, 2012, **4**, 5826–5834.
4 J. Lu, J. W. Elam and P. C. Stair, *Acc. Chem. Res.*, 2013, **46**, 1806–1815.
5 Y. S. Jeong, J.-B. Park, H.-G. Jung, J. Kim, X. Luo, J. Lu, L. Curtiss, K. Amine, Y.-K. Sun, B. Scrosati and Y. J. Lee, *Nano Lett.*, 2015, **15**, 4261–4268.
6 Y. Wu, H. Yu, H. Wang and F. Peng, *Chin. J. Catal.*, 2014, **35**, 952–959.
7 S. Padalkar, J. R. Capadona, S. J. Rowan, C. Weder, Y.-H. Won, L. A. Stanciu and R. J. Moon, *Langmuir*, 2010, **26**, 8497–8502.
8 T. Kamal, I. Ahmad, S. B. Khan and A. M. Asiri, *Int. J. Biol. Macromol.*, 2019, **135**, 1162–1170.
9 F. Jiao, J. Wang, Y. Lin, J. Li, X. Jing and Y. Gong, *Appl. Surf. Sci.*, 2021, **553**, 149440.
10 K. Saravanakumar, V. S. Priya, V. Balakumar, S. L. Prabavathi and V. Muthuraj, *Environ. Res.*, 2022, **212**, 113185.
11 J. C. Védrine, *Catalysts*, 2017, **7**, 341.
12 R. Tao, X. Ma, X. Wei, Y. Jin, L. Qiu and W. Zhang, *J. Mater. Chem. A*, 2020, **8**, 17360–17391.
13 D. Chen, H. Feng and J. Li, *Chem. Rev.*, 2012, **112**, 6027–6053.

14 L. Saikam, P. Arthi, B. Senthil and M. Shanmugam, *Inorg. Chem. Commun.*, 2023, **152**, 110685.
15 W. S. Hummers Jr. and R. E. Offeman, *J. Am. Chem. Soc.*, 2002, **80**, 1339.
16 A. Jiříčková, O. Jankovský, Z. Sofer and D. Sedmidubský, *Materials*, 2022, **15**, 920.
17 Y. Tian, Z. Yu, L. Cao, X. L. Zhang, C. Sun and D.-W. Wang, *J. Energy Chem.*, 2021, **55**, 323–344.
18 C. Kavitha, *Mater. Today: Proc.*, 2022, **49**, 811–816.
19 W. Zhang, H. Xu, F. Xie, X. Ma, B. Niu, M. Chen, H. Zhang, Y. Zhang and D. Long, *Nat. Commun.*, 2022, **13**, 471.
20 M. J. Ndolomingo, N. Bingwa and R. J. Meijboom, *J. Mater. Sci.*, 2020, **55**, 6195–6241.
21 P. Arranz-Mascaros, M. L. Godino-Salido, R. Lopez-Garzon, C. García-Gallarín, I. Chamorro-Mena, F. J. Lopez-Garzon, E. Fernandez-García and M. D. Gutierrez-Valero, *ACS Omega*, 2020, **5**, 18849–18861.
22 L. Xin, F. Yang, S. Rasouli, Y. Qiu, Z.-F. Li, A. Uzunoglu, C.-J. Sun, Y. Liu, P. Ferreira, W. Li, Y. Ren, L. A. Stanciu and J. Xie, *ACS Catal.*, 2016, **6**, 2642–2653.
23 S. Gupta and R. Meek, *Sens. Actuators, B*, 2018, **274**, 85–101.
24 Y. Y. Khine, X. Wen, X. Jin, T. Foller and R. Joshi, *Phys. Chem. Chem. Phys.*, 2022, **24**, 26337–26355.
25 H. Hsu, J. Bugno, S. Lee and S. Hong, *Rev. Nanomed. Nanobiotechnol.*, 2017, **9**, e1409.
26 D. A. Tomalia, *Prog. Polym. Sci.*, 2005, **30**, 294–324.
27 J. M. J. Frechet, *Science*, 1994, **263**, 1710–1715.
28 D. Balamurugan, P. P. Arun and B. Karel, *Coord. Chem. Rev.*, 2021, **444**, 214062.
29 R. Rajmohan, L. Kannappan and S. Mari, *New J. Chem.*, 2021, **45**, 14227–14235.
30 Z. Weiguang, Z. Xiaofei, K. Mengxin, X. Jingyi, Z. Yinxiu, S. Mi, Z. Chao and L. Hong, *J. Electroanal. Chem.*, 2022, **912**, 116254.
31 C. C. Lee, J. A. MacKay, J. M. J. Fréchet and F. C. Szoka, *Nat. Biotechnol.*, 2005, **23**, 1517–1526.
32 S. Svenson and D. A. Tomalia, *Adv. Drug Delivery Rev.*, 2012, **64**, 102–115.
33 H. Irshad, M. Nadeem, S. Qamar, S. Dan, J. Micong, Y. Liu, L. Gan, W. Xu, I. Azeem and Y. Zhu, *TrAC, Trends Anal. Chem.*, 2022, **157**, 116810.
34 F. Tiago, L. Daniel-da-Silva and T. Tito, *Coord. Chem. Rev.*, 2022, **460**, 214483.
35 N. Faezeh, G. Naser, S. Mehdi and S.-K. Mehdi, *J. Phys. Chem. Solids*, 2021, **148**, 109682.
36 I. J. Majoros, T. P. Thomas, C. B. Mehta and J. R. Baker, *J. Med. Chem.*, 2005, **48**, 5892–5899.
37 W. B. Turnbull and J. F. Stoddart, *Rev. Mol. Biotechnol.*, 2002, **90**, 231–255.
38 A. Kommu, V. Velachi, M. N. D. S. Cordeiro and J. K. Singh, *J. Phys. Chem. A*, 2017, **121**, 9320–9329.
39 L. Dai, D. W. Chang, J. Baek and W. Lu, *Small*, 2012, **8**, 1130–1166.
40 A. P. Abbott, G. Capper, D. L. Davies, R. K. Rasheed and V. Tambyrajah, *Chem. Commun.*, 2003, 70–71.
41 C. M. Q. Le, X. T. Cao, T. T. K. Tu, W. K. Lee and K. T. Lim, *Appl. Surf. Sci.*, 2018, **450**, 122–129.
42 P. Torres, M. Balcells and R. Canela-Garayoa, *ACS Omega*, 2021, **6**, 19392–19399.
43 T. N. T. Nguyen, N. T. Pham, D.-H. Ngo, S. Kumar and X. T. Cao, *ACS Omega*, 2023, **8**, 25385–25391.
44 J. R. Morones, J. L. Elechiguerra, A. Camacho, K. Holt, J. B. Kouri, J. T. Ramirez and M. J. Yacaman, *Nanotechnology*, 2005, **16**, 2346–2353.
45 M. Rai, A. Yadav and A. Gade, *Biotechnol. Adv.*, 2009, **27**, 76–83.
46 J. S. Kim, E. Kuk, K. N. Yu, J. H. Kim, S. J. Park, H. J. Lee, S. H. Kim, Y. K. Park, Y. H. Park, C.-Y. Hwang, Y.-K. Kim, Y.-S. Lee, D. H. Jeong and M. H. Cho, *Nanomed.: Nanotechnol. Biol. Med.*, 2007, **3**, 95–101.
47 M. Rai, A. P. Ingle, S. Birla, A. Yadav and C. A. D. Santos, *Crit. Rev. Microbiol.*, 2012, **38**, 313–336.